Accounting for Non-stationarity in Extreme Snow Loads: a Comparison with Building Standards in the French Alps

Erwan Le Roux[1], Guillaume Evin[1], Nicolas Eckert[1], Juliette Blanchet[2], and Samuel Morin[3]

[1]Univ. Grenoble Alpes, INRAE, UR ETNA
[2]Univ. Grenoble Alpes, Grenoble INP, CNRS, IRD, IGE
[3]Univ. Grenoble Alpes, Univ. Toulouse, Météo-France, CNRS, CNRM, CEN Grenoble

Correspondence: Erwan Le Roux (erwan.le-roux@inrae.fr)

Abstract. In a context of climate change, trends in extreme snow loads need to be determined to minimize the risk of structure collapse. We study trends in annual maxima of ground snow load (GSL) using non-stationary extreme value models. Trends in return levels of GSL are assessed at a mountain massif scale from GSL data, provided for the French Alps from 1959 to 2019 by a meteorological reanalysis and a snowpack model. Our results indicate a temporal decrease in 50-year return levels

5   from 900 m to 4200 m, significant in the Northwest of the French Alps until 2100 m. Despite this decrease, in half of the massifs, the return level in 2019 at 1800 m exceeds the return level designed for French building standards under a stationary assumption. We believe that this high number of exceedances is due to questionable assumptions concerning the computation of current standards. For example, these were devised with GSL, estimated from snow depth and constant snow density set to 150 kg m^{-3}, which underestimate typical GSL values for the full snowpack.

1 Introduction

10

Extreme snow loads can generate economic damages and casualties. For instance, more than \$200 million in roof damages occurred during the Great Blizzard of 1993 (O'Rourke and Auren, 1997). Recently, at the Katowice International Fair in 2006, the roof of one of the buildings collapsed under a layer of snow, leading to 65 casualties and 140 injured (BBC News, 2006). In France, snow loads over Roussillon in 1986, caused both 17 million euros in damages and a major power outage due to

15   overloading of electrical cables and pylons by sticking snow (Vigneau, 1987; Naaim-Bouvet et al., 2000).

Ground snow load (GSL) is defined as the pressure exerted by accumulated snow on the ground, which can be directly associated to accumulated snow on structures, e.g. on roofs (Sanpaolesi et al., 1998). In details, the observed height of accumulated snow is called snow depth (in m). The density of this snow can vary widely between precipitation particles ($\rho_{\text{SNOW}} \approx 100$ kg m^{-3}) and a ripe snowpack ($\rho_{\text{SNOW}} \approx 500$ kg m^{-3}). Multiplying snow depth by snow density gives the sur-

20   facic mass of snow (in kg m^{-2}). Surfacic mass of snow corresponds to the snow water equivalent which is the height of water (in mm) we could obtain if we melt all the snow in a 1 m^2 area. Indeed, since water density is $\rho_{\text{WATER}} = 1000$ kg m^{-3}, we have that 1 mm of water on 1 m^2 has a surfacic mass of 1 kg m^{-2}. Snow load is the pressure exerted by this surfacic mass of snow (in N m^{-2} or Pa) and equals the snow water equivalent times the gravitational acceleration (g = 9.81 m s^{-2}).

Snowpack variables related to GSL (snow depth, snow water equivalent) evolve with climate change. As shown in Table 1,
25 literature on past trends in snowpack variables for the Western Alps shows a decreasing trend. Literature on projected trends also
points to a decrease (stronger for the second half of the 21st century under a high greenhouse gas emission scenario than with
strong reductions in greenhouse gas emissions) for mean winter (December-May) snow water equivalent in the European Alps
(IPCC, 2019). However, anthropogenic climate change impacts climatic variables in their averages, but also in their extremes
(G Klein Tank and K Nnen, 2003; IPCC, 2012). For instance, annual maxima of snow depth have decreased in Switzerland
30 (Marty and Blanchet, 2012). Projected trends in extreme snowpack variables are prone to strong uncertainties (Strasser, 2008;
Beniston et al., 2018) as both mean winter temperature (IPCC, 2019) and winter precipitation extremes (Rajczak and Schär,
2017) are projected to increase in the European Alps.

Variable	Indicator	Trend	Country	Time	Source
HS	Seasonal mean (Nov to Apr)	Decrease	CH	1931-1999	Laternser and Schneebeli (2003)
	Winter mean (Dec to Feb)	Decrease in the North	FR	1958-2007	Durand et al. (2009b)
	Mean annual maxima	Decrease	CH	1930-2010	Marty and Blanchet (2012)
	Seasonal mean (Nov to May)	Decrease	IT	1951-2010	Terzago et al. (2013)
	Seasonal mean (Nov to Apr)	Decrease in the South	CH	1961–2012	Schöner et al. (2019)
SWE	1st of April value	Decrease	IT	1965-2007	Bocchiola and Diolaiuti (2010)
	1st of April value	Decrease	FR, IT, CH	1968-2012	Marty et al. (2017)

Table 1. Past trends in snow depth (HS) and snow water equivalent (SWE) according to existing studies in the Western Alps, i.e. in Italy
(IT), France (FR), and Switzerland (CH). In the trend column, "North" and "South" refer to the considered country.

The impact of climate change on GSL was not taken into account in current European standards for structural design, a.k.a
Eurocodes (Sanpaolesi et al., 1998), which drive French standards (Biétry, 2005). These standards define that structures must
35 withstand their own weight plus a pressure proportional to a characteristic value. The latter is the stationary 50-year return
level of GSL, i.e. exceeded once every 50 years in average. Thus, studying trends in 50-year return levels of GSL is needed
for updating these standards (Croce et al., 2018). In the literature, past and projected trends in 50-year return levels of GSL
have rarely been investigated with the exception of (Rózsás et al., 2016; Il Jeong and Sushama, 2018; Croce et al., 2018). In
the French Alps, several studies focused on extreme snow variables (Biétry, 2005; Gaume et al., 2012, 2013) and their spatial
40 dependence (Nicolet et al., 2015, 2016, 2017, 2018). However, trends in 50-year return levels of GSL remain unexplored.
We fill these gaps by studying annual maxima of GSL provided every 300 m of elevation at a mountain massif scale for the
23 French Alps massifs. We rely on a reanalysis produced by the SAFRAN-Crocus chain (Durand et al., 2009a; Vionnet et al.,
2012) available for the period 1959-2019. The major advantage of this reanalysis is to take benefit of an advanced snowpack
model which provides daily estimates of ground snow load values, while previous studies relied on approximate values directly
45 related to snow depth with a crude estimation of snow density (Biétry, 2005). Our methodology consists in applying stationary
and non-stationary extreme value models to annual maxima time series. We select one model by massif and altitude with the
AIC statistical criterion, and assess its significance with the likelihood ratio statistical test. Finally, for each massif and altitude,

Natural Hazards
and Earth System
Sciences
Discussions

we compute the relative change in 50-year return level between 1960 and 2010, and we compare the non-stationary return
level in 2019 with the stationary return level designed for French building standards. Our approach considers only natural snow
50 processes, i.e. we do not account for snow removal throughout the year and consider all processes (accumulation, thaw/freeze,
melt, compaction etc.) occurring during the winter season.

This paper is organized as follows. Section 2 presents our data. Section 3 describes standards for ground snow load. Then,
section 4 explains our methodology. Results, discussion and conclusions are introduced in Sections 5, 6 and 7, respectively.

2 Ground snow load data

55 The study area covers the French Alps which are located between Lake Geneva to the north and the Mediterranean Sea to the
south (Fig. 1). The climate is contrasted, colder and wetter in the northern Alps and much drier in the southern Alps (Durand
et al., 2009a). This region is typically divided into 23 mountain massifs. In this work, we rely on a reanalysis (Vernay et al.,
2019) from the SAFRAN-Crocus chain (Durand et al., 2009a; Vionnet et al., 2012) available from August 1958 to July 2019
at the scale of these massifs, for 300 m elevation bands from 300 m to 4800 m. However, annual maxima are only available
60 from 1959 to 2019. Indeed, in this work, annual maxima denotes the maxima during a year centered on the winter season, e.g.
annual maxima for the year 1959 correspond to the maxima from the 1st of August 1958 to the 31st of July 1959.
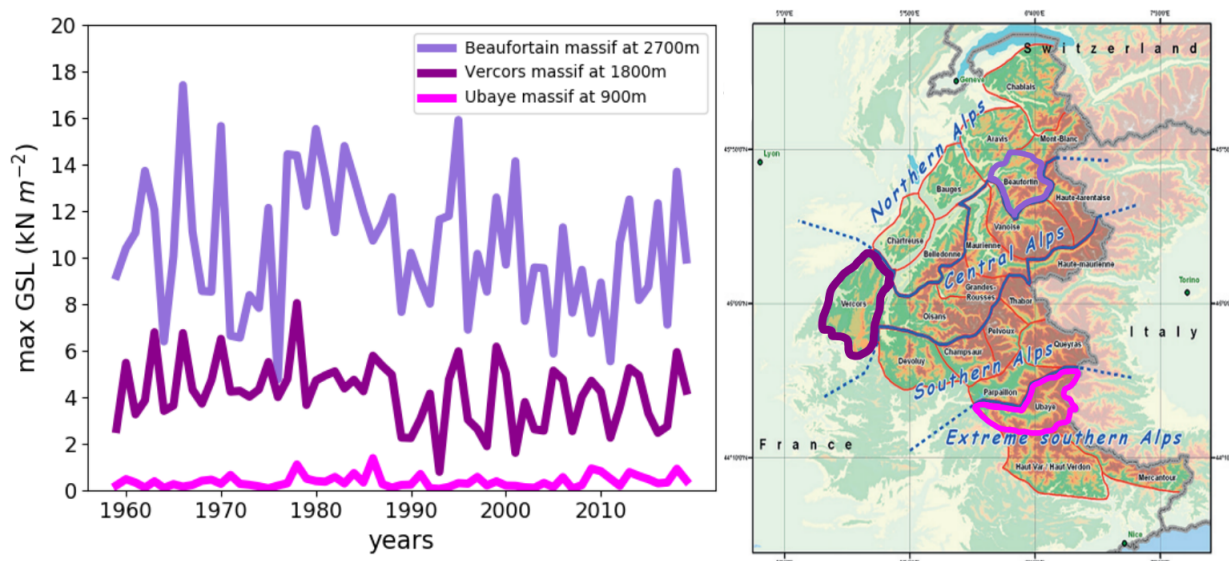

Figure 1. Left: Three time series of annual maxima for ground snow load (GSL) from 1959 to 2019 for 3 massifs at low (900 m), mid (1800 m) or high (2700 m) altitude. Right: 23 mountains massifs of the French Alps and their orographic features (Durand et al., 2009a).

SAFRAN meteorological reanalysis (Durand et al., 2009a) provides consistent meteorological data (precipitation, temperature, humidity, radiation, wind speed) over the considered mountain massifs and elevations. The Crocus snowpack model
(Vionnet et al., 2012) infers snow depth and snow water equivalent (SWE) based on SAFRAN time series. Crocus is a one-

65 dimensional multilayer physical snow scheme, which simulates the snowpack evolution over time, by accounting for several processes such as thermal diffusion, phase changes and metamorphism. A large intercomparison of snow models illustrates that Crocus is among the top models to simulate SWE (Krinner et al., 2018). Furthermore, another recent intercomparison of SWE products emphasizes Crocus usefulness as it concludes that ensembles containing Crocus (and/or Crocus driven by ERA-Interim reanalysis) perform better than those that do not (Mortimer et al., 2019).

70 In this paper, GSL equals the SWE from the SAFRAN-Crocus chain times the gravitational acceleration. We study time series of annual maxima of GSL for each massif from 1959 to 2019 for 300 m elevation bands from 300 m to 4800 m (Fig. 1).

3 Standards for ground snow load in the French Alps

GSL French standards (Biétry, 2005) are based mostly on Eurocodes (Sanpaolesi et al., 1998) and on prior French standards (AFNOR, 1996). Each French department, and by extension each French Alps massif, is associated with a region (C or E) that
75 sets characteristic 50-year return level values of GSL between 200 m and 2000 m of altitude (Fig. 2).
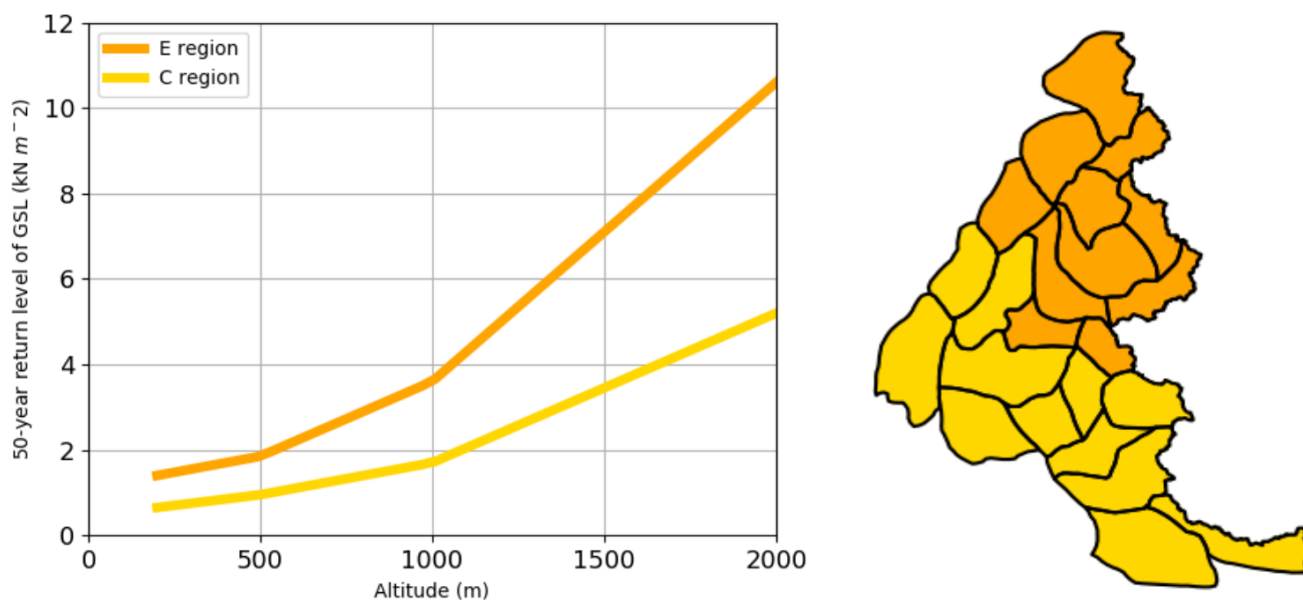

Figure 2. Left: French standards 50-year return levels of ground snow load (GSL) w.r.t the altitude for regions C and E. Right: Regions map.

French standards were elaborated with annual maxima time series of snow depth on the ground measured in stations from 1945 to 1992. GSL data were approximated from annual maxima of snow depth and by assuming that snow density equals $150\,\mathrm{kg\,m^{-3}}$. Following Eurocodes, characteristic value of GSL is defined as the 50-year return level of a Gumbel distribution (Sect. 4.1). This distribution was fitted using the least squares method and by removing the top annual maximum when
80 considered exceptional (Biétry, 2005).

4 Statistical Methodology

Following extreme value theory, we employ 2 stationary models and 6 non-stationary models for time series of annual maxima of GSL (Sect. 4.1). We select a single model for each time series (i.e. for each massif and altitude) with the AIC statistical criterion, and assess its significance with the likelihood ratio statistical test (Sect. 4.2). Finally, we compute the relative change in 50-year return levels of GSL, and quantify their uncertainty (Sect. 4.3).

4.1 Stationary and non-stationary models based on extreme value distributions

Climate extremes are generally studied with statistics. As underlined in the IPCC special report on climate extremes, a large amount of statistical literature builds on extreme indices to examine moderate extremes (IPCC, 2012). However, since we focus on rarer extremes, it is recommended to rely on extreme value theory (EVT) (Coles, 2001). Such statistical models provide and hypothesize additional prior information in order to compensate the limited amount of empirical observations that commonly span only several decades. These models can be used to extrapolate beyond the empirical observations, and to estimate return levels (Sect. 4.3).

EVT offers a suitable framework to analyse extreme values, i.e. to model the form of the tail for almost any probability distribution. Asymptotically, as the central limit theorem motivates sample means modelling with the normal distribution, the Fisher–Tippett–Gnedenko theorem (Fisher and Tippett, 1928; Gnedenko, 1943) encourages sample maxima modelling with the GEV distribution. This theorem justifies that the maximum of finite-sized blocks with a large enough block size can be modeled with the GEV distribution. In practice, an annual maximum is thus usually considered as a realization of a GEV distribution. Three parameters define the GEV distribution: a location μ, a scale $\sigma > 0$ and a shape ζ (a.k.a extremal index or tail index). The GEV distribution includes three specific types of distributions: Weibull ($\zeta < 0$), Fréchet ($\zeta > 0$) and Gumbel ($\zeta = 0$). Thus, by definition, if Y represents annual maximum of GSL, we can assume that Y follows a GEV distribution, i.e. $Y \sim \text{GEV}(\mu, \sigma, \zeta)$, which implies that:

$$P(Y \leq y) = \begin{cases} \exp\left[-(1 + \zeta\frac{y-\mu}{\sigma})_+^{-\frac{1}{\zeta}}\right] \text{ if } \zeta \neq 0 \text{ and where } u_+ \text{ denotes } \max(u, 0), \\ \exp\left[-\exp\left(-\frac{y-\mu}{\sigma}\right)\right] \text{ if } \zeta = 0, \text{ in other words if } Y \sim \text{Gumbel}(\mu, \sigma). \end{cases} \quad (1)$$

In a context of climate change, a large amount of hydrological literature builds on non-stationary modelling (Milly et al., 2008) to assess whether a time series is generated by a unique probability distribution (stationary model), or if the generating probability distribution is changing (non-stationary model). Non-stationary extremes are usually studied with both non-stationary modelling and EVT (Katz et al., 2002). Annual maxima are assumed independent but not necessarily identically distributed (Serinaldi and Kilsby, 2015). Such approaches combine a stationary random component (a fixed extreme value distribution) with non-stationary deterministic functions that map each temporal covariate t to the changing parameters of the distribution (Montanari and Koutsoyiannis, 2014). In a non-stationary context, Zhang et al. (2004) showed that tests based on this parametric approach have stronger power of detection when compared with non-parametric methods.

In this paper, we consider non-stationarity for both the Gumbel distribution and the more general GEV distribution, since they represent natural extensions of the Gumbel distribution which was used for French building standards (Sect. 3). For any model, we have that $Y(t) \sim \text{GEV}(\mu(t), \sigma(t), \zeta(t))$, as the Gumbel distribution correspond to $\zeta(t) = 0$. For a model $\mathcal{M}$, we denote as $\boldsymbol{\theta_{\mathcal{M}}}$ all parameters for its functions ($\mu(t)$, $\sigma(t)$ and $\zeta(t)$). We focus on simple linear functions due to the limited

115 length of time series (60 years). The linearity starts in 1959 which is the first winter with available data. As shown in Table 2, we consider only models with a constant shape parameter, but where the location and/or the scale parameter can vary linearly with years t.

Model type	Distribution	Model name	$\mu(t)$	$\sigma(t)$	$\zeta(t)$	$\boldsymbol{\theta_{\mathcal{M}}}$	# $\boldsymbol{\theta_{\mathcal{M}}}$
Stationary	Gumbel	$\mathcal{M}_0$	μ_0	σ_0	0	(μ_0, σ_0)	2
	GEV	$\mathcal{M}_{\zeta_0}$			ζ_0	$(\mu_0, \sigma_0, \zeta_0)$	3
Non-stationary	Gumbel	$\mathcal{M}_{\mu_1}$	$\mu_0 + \mu_1 \times (t - 1959)$	σ_0	0	(μ_0, μ_1, σ_0)	3
	GEV	$\mathcal{M}_{\zeta_0, \mu_1}$			ζ_0	$(\mu_0, \mu_1, \sigma_0, \zeta_0)$	4
Non-stationary	Gumbel	$\mathcal{M}_{\sigma_1}$	μ_0	$\sigma_0 + \sigma_1 \times (t - 1959)$	0	$(\mu_0, \sigma_0, \sigma_1)$	3
	GEV	$\mathcal{M}_{\zeta_0, \sigma_1}$			ζ_0	$(\mu_0, \sigma_0, \sigma_1, \zeta_0)$	4
Non-stationary	Gumbel	$\mathcal{M}_{\mu_1, \sigma_1}$	$\mu_0 + \mu_1 \times (t - 1959)$	$\sigma_0 + \sigma_1 \times (t - 1959)$	0	$(\mu_0, \mu_1, \sigma_0, \sigma_1)$	4
	GEV	$\mathcal{M}_{\zeta_0, \mu_1, \sigma_1}$			ζ_0	$(\mu_0, \mu_1, \sigma_0, \sigma_1, \zeta_0)$	5

Table 2. Statistical models considered for annual maxima of GSL are based on the Gumbel or the GEV distribution, and are extensions of the stationary Gumbel model. For non-stationary models, the location and/or the scale vary linearly with years t after the starting year 1959.

4.2 Model selection

Let $\boldsymbol{y} = (y_{1959}, ..., y_{2019})$ represents a time series of annual maxima of GSL, i.e. for a massif and an elevation band (Sect.
120 2). First, models are fitted with the maximum likelihood method. For every model $\mathcal{M}$, we compute the maximum likelihood estimator $\widehat{\boldsymbol{\theta}}_{\mathcal{M}}$ which corresponds to the parameter $\boldsymbol{\theta_{\mathcal{M}}}$ that maximizes the likelihood:

$$\widehat{\boldsymbol{\theta}}_{\mathcal{M}} = \underset{\boldsymbol{\theta_{\mathcal{M}}}}{\text{argmax}} \, \mathcal{L}(\boldsymbol{\theta_{\mathcal{M}}}; \boldsymbol{y}) \text{ where } \mathcal{L}(\boldsymbol{\theta_{\mathcal{M}}}; \boldsymbol{y}) = p(\boldsymbol{y}|\boldsymbol{\theta_{\mathcal{M}}}) = \prod_t p(y_t|\mu(t), \sigma(t), \zeta(t)) = \prod_t \frac{\partial P(Y(t) \leq y_t)}{\partial y_t}. \quad (2)$$

Then, for each $\boldsymbol{y}$, i.e. for each massif and elevation band, we select the model $\mathcal{M}_N$ with the minimal AIC value (Akaike, 1974), as it is the best information criterion in a non-stationary context with small sample sizes (Kim et al., 2017). We define
125 that:

$$\mathcal{M}_N = \underset{\mathcal{M} \in \text{Table 2}}{\text{argmin}} \, \text{AIC}(\mathcal{M}) \text{ where } \text{AIC}(\mathcal{M}) = 2 \times [\#\boldsymbol{\theta_{\mathcal{M}}} - \log \mathcal{L}(\widehat{\boldsymbol{\theta}}_{\mathcal{M}}; \boldsymbol{y})], \text{ where } \#\boldsymbol{\theta_{\mathcal{M}}} \text{ is the cardinality of } \boldsymbol{\theta_{\mathcal{M}}}. \quad (3)$$

The selected model $\mathcal{M}_N$ can be any model from Table 2, i.e. a stationary or a non-stationary model. The subscript N designates the number of additional parameters compared to the stationary Gumbel model $\mathcal{M}_0$, i.e. $N = \#\boldsymbol{\theta}_{\mathcal{M}_N} - \#\boldsymbol{\theta}_{\mathcal{M}_0}$.

Natural Hazards
and Earth System
Sciences

Open Access

EGU

Discussions

130 If $\mathcal{M}_N$ is not the model $\mathcal{M}_0$ then, since models are nested, we can compute the significance of $\mathcal{M}_N$ w.r.t $\mathcal{M}_0$ with a likelihood ratio test (Coles, 2001). This test assess whether there is enough evidence to move from the stationary Gumbel model $\mathcal{M}_0$ to the selected model $\mathcal{M}_N$. The null hypothesis can be stated as: the N additional parameters of the model $\mathcal{M}_N$ can be set to zero. In other words, we want to check if setting to zero the N additional parameters of the model $\mathcal{M}_N$ is supported by the data $\boldsymbol{y}$. Under the null hypothesis, the likelihood ratio test statistic (LR) has an asymptotic χ^2_N-distribution: $\mathrm{LR}(\widehat{\boldsymbol{\theta}}_{\mathcal{M}_N}, \widehat{\boldsymbol{\theta}}_{\mathcal{M}_0}, y) = 2\log\frac{\mathcal{L}(\widehat{\boldsymbol{\theta}}_{\mathcal{M}_N}: \boldsymbol{y})}{\mathcal{L}(\widehat{\boldsymbol{\theta}}_{\mathcal{M}_N}: \boldsymbol{y})} \dot{\sim} \chi^2_N$, where $\dot{\sim}$ means distributed under suitable regularity conditions.

135 In practice, the test works as follows. We first choose a 0.05 level of significance. Then, if LR is greater than $q_{\chi^2_N}$, the $1 - 0.05 = 0.95$ quantile of the χ^2_N distribution, it means that we reject the nested model $\mathcal{M}_0$ in favor of the selected model $\mathcal{M}_N$. In this case, if the selected model $\mathcal{M}_N$ is non-stationary, then we consider the associated trend as significant.

4.3 Return level

In a stationary context, the T-year return level, which corresponds to a return period of T years, is the classical metric to
140 quantify hazards of extreme events (Cooley, 2012). For a stationary model, there is a one-to-one relationship between a return level (a quantile exceeded each year with probability p) and a return period (a duration exceeded every $T = \frac{1}{p}$ years in average).

In a non-stationary context, return level and return period concepts (Cooley, 2012) become further ambiguous, prone to misconceptions and can lead to misleading conclusions (Serinaldi, 2015). We focus on the yearly level for a fixed probability of exceedance, a.k.a effective return level (Katz et al., 2002; Cheng et al., 2014), as it conveys best that hazard evolves with time.

145

For the stationary Gumbel model $\mathcal{M}_0$, the return level $z_p(\boldsymbol{\theta}_{\mathcal{M}_0})$ is defined as the level exceeded each year with probability p. In other words, if Y denotes an annual maximum, then $P(Y \leq z_p(\boldsymbol{\theta}_{\mathcal{M}_0})) = 1 - p$. This return level is constant through time and equals $z_p(\boldsymbol{\theta}_{\mathcal{M}_0}) = \mu_0 - \sigma_0 \log(-\log(1 - p))$. In this paper, we set $p = \frac{1}{50} = 0.02$ as it corresponds to the 50-year return period defined by French standards (based on European standards) for the design working life of buildings (Sect. 3).

150 For the selected model $\mathcal{M}_N$, we define our return level as the yearly level for a fixed probability of exceedance p. For any model considered in Table 2, we obtain that $z_p(\boldsymbol{\theta}_{\mathcal{M}_N}, t) = \mu_0 + \mu_1 \times (t - 1959) - \frac{\sigma_0 + \sigma_1 \times (t - 1959)}{\zeta_0}[1 - (-\log(1 - p))^{-\zeta_0}]$, where we set μ_1, σ_1 or ζ_0 to 0 if they are not defined in the model $\mathcal{M}_N$. For example, for the Gumbel model $\mathcal{M}_0$, the return level is constant: for any year t, $z_p(\boldsymbol{\theta}_{\mathcal{M}_0}, t) = \lim_{\zeta_0 \to 0}[\mu_0 + \frac{\sigma_0}{\zeta_0}(1 - (-\log(1 - p))^{-\zeta_0})] = \mu_0 - \sigma_0 \log(-\log(1 - p))$.

For any considered model, the time derivative of the return level is constant, as $\frac{\partial z_p(\boldsymbol{\theta}_{\mathcal{M}_N}, t)}{\partial t} = \mu_1 - \frac{\sigma_1}{\zeta_0}(1 - (-\log(1 - p))^{-\zeta_0})$.
155 It quantifies the yearly change in return level. Thus, the relative difference of return levels between year t_1 and year t_2 is:

$$\text{Relative change}(z_p(\boldsymbol{\theta}_{\mathcal{M}_N}, t_1), z_p(\boldsymbol{\theta}_{\mathcal{M}_N}, t_2)) = \frac{z_p(\boldsymbol{\theta}_{\mathcal{M}_N}, t_2) - z_p(\boldsymbol{\theta}_{\mathcal{M}_N}, t_1)}{z_p(\boldsymbol{\theta}_{\mathcal{M}_N}, t_1)} = \frac{t_2 - t_1}{z_p(\boldsymbol{\theta}_{\mathcal{M}_N}, t_1)} \times \frac{\partial z_p(\boldsymbol{\theta}_{\mathcal{M}_N}, t)}{\partial t}. \qquad (4)$$

In the context of maximum likelihood estimation, uncertainty related to return levels can be derived by the delta method, which quickly provides confidence intervals both in the stationary and non-stationary case (Coles, 2001; Gilleland and Katz, 2016). First, the return level estimator associated to the maximum likelihood estimator simply equals $z_p(\widehat{\boldsymbol{\theta}}_{\mathcal{M}})$. Then, due to
160 the asymptotic normality of the maximum likelihood estimator (MLE), we can assume that, even with a finite number of data,

the MLE is normally distributed. Therefore, we have that under regularity conditions, limits of the $1 - \alpha = 95\%$ confidence interval are $\widehat{\boldsymbol{\theta}}_{\mathcal{M}} \pm q_{\frac{\alpha}{2}} \times v_{z_p}(\widehat{\boldsymbol{\theta}}_{\mathcal{M}})$ where $q_{\frac{\alpha}{2}}$ is the 1-$\frac{\alpha}{2}$ quantile of the standard normal distribution, and v_{z_p} is a function that associates to each parameter $\boldsymbol{\theta}_{\mathcal{M}}$ the variance of the approximate normal distribution associated to its return level $z_p(\boldsymbol{\theta}_{\mathcal{M}})$. For a full expression of the function v_{z_p} and for details on the delta method, we refer to Theorem 2.4 of Coles (2001). In particular,

165 this theorem explains that the delta method is valid for $\zeta_0 < 1$, which is respected in our case as $-0.5 \leq \zeta_0 \leq 0.5$ (Sect. 5). Also, uncertainty of non-stationary return levels $z_p(\widehat{\boldsymbol{\theta}}_{\mathcal{M}}, t)$ can be obtained by incorporating the covariate t in the function z_p.

4.4 Application

First, we exclude 4 times series of annual maxima with more than 10% of zeros, i.e. years without GSL. Then, we fit models on time series, and retain only those with $-0.5 \leq \widehat{\zeta}_0 \leq 0.5$. This impacts 3 time series. We made this choice because $\widehat{\zeta}_0 > 0.5$

170 designates distributions with an "exploding" tail which are known to be physically implausible (Martins and Stedinger, 2000). We select one model for each time series (i.e. for each massif and altitude) with the AIC statistical criterion, and assess its significance with the likelihood ratio test (Sect. 4.2).

5 Result

5.1 Selected models

175 Figure 3 shows that a stationary model, i.e. models $\mathcal{M}_0$ and $\mathcal{M}_{\zeta_0}$, is selected for a majority (57%) of time series studied (Sect. 2). Models with a linearity in both the location and scale parameters are the most frequently selected non-stationary models (22%). For both stationary and non-stationary models, Gumbel models are always more selected that their corresponding GEV models (Fig. 3, Fig. 4). All in all, we highlight that 40% of selected models are significantly different from the stationary Gumbel model $\mathcal{M}_0$.
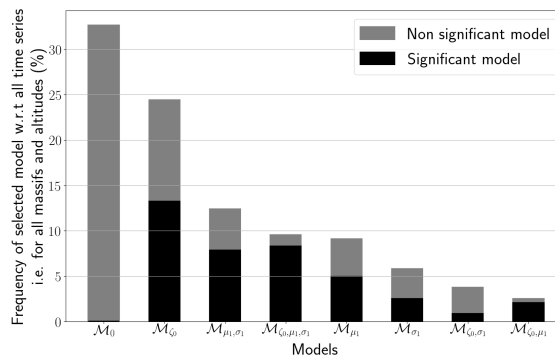

Figure 3. Distribution of selected models. Frequency of selected model (in %) w.r.t all time series, i.e. for all massifs and altitudes. For the selection procedure and the definition of significance, we refer to Sect. 4.2.

180   Figure 4 depicts shape parameter values for the selected model at 900 m, 1800 m and 2700 m. We notice that a majority of
massifs are white-colored illustrating that a (stationary or non-stationary) Gumbel model (i.e. $\widehat{\zeta_0} = 0$) is selected (Sect. 5). It
emphasizes that a Gumbel distribution often explains more succinctly the data than a GEV distribution. Also, with the GEV
distribution, the estimated most likely shape parameter $\widehat{\zeta_0}$ is often quite uncertain, i.e. confidence intervals are large, which is
the main reason why French standards did not rely on it. This uncertainty comes from the limited length of time series, and
185   longer time series would certainly reduce it, and thus estimate the most likely shape parameter more robustly.

On Figure 4, we further observe that non-null shape parameters at low altitudes ($\leq$ 900 m) are always positive (brown-
colored massifs), i.e. a Fréchet distribution is preferred. On the other hand, for high altitudes ($\geq$ 1500 m) non-null shape
parameters are always negative (green-colored massifs), i.e. a Weibull distribution is favored. We hypothesize that this might
be due to the different nature of annual maxima of GSL between low and high altitudes. At high altitudes, annual maxima
190   are mainly due to snowpack accumulation during several months, while at low altitudes this accumulation is limited, and thus
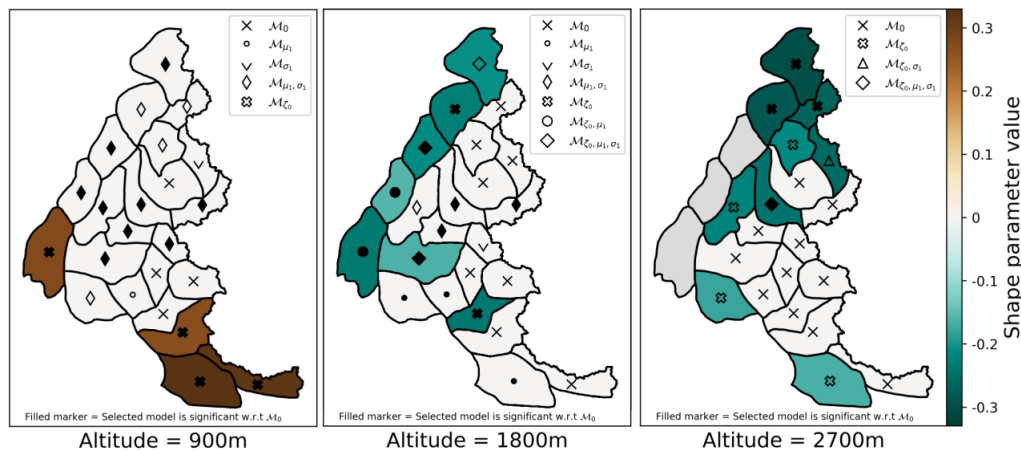annual maxima roughly correspond to heavy precipitations.

Figure 4. Shape parameter values for the selected model at low (900 m), mid (1800 m) or high (2700 m) altitude. Markers show selected
model $\mathcal{M}_\mathcal{N}$. Filled markers symbolize significant trend. For the selection procedure and the definition of significance, we refer to Sect. 4.2.

5.2   Trends in return levels of ground snow load

Figure 5 maps the relative change between 1960 and 2010 for 50-year return levels of GSL at 900 m, 1800 m and 2700 m
(see App. A for maps at all altitudes). Quantitatively, for Northwest massifs, we observe that return levels have decreased
195   by up to 60% at 900 m (dark blue), while at 1800 m this decrease is less marked (pale blue). Qualitatively, these decreasing
trends are frequently due to significant changes both in the location and scale parameters of the Gumbel or GEV distribution
(diamond-shaped filled markers). At 2700 m, or in the South at 900 m and 1800 m, no trends are found (white color), since
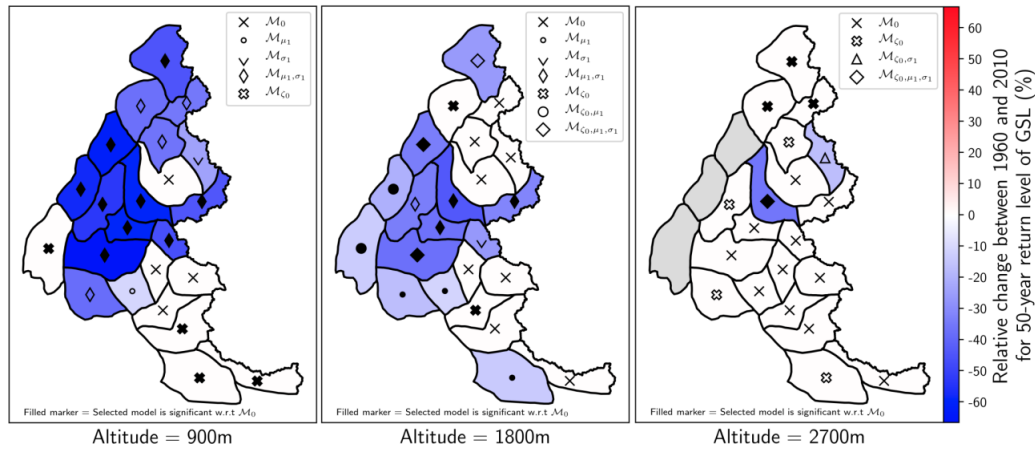stationary models are often selected (cross-shaped markers).

Figure 5. Trends in 50-year return levels of ground snow load (GSL) at low (900 m), mid (1800 m) or high (2700 m) altitude. Markers show selected model $\mathcal{M}_N$. Filled markers symbolize significant trend. Colors illustrate relative change for 50-year non-stationary return levels of GSL between 1960 and 2010. For the selection procedure and the definition of significance, we refer to Sect. 4.2.

Figure 6 emphasizes the evolution of decreasing trends between 900 m and 4800 m of altitude. We observe that decreasing

200   trends are significant for more than one-third of the massifs, located in the Northwest of the Alps (Sect. A), until 2100 m (black bars). In half a century, return levels have dropped in average by up to 30% at 900 m. At higher altitudes we observe a decline in the percentage of massifs with a significant decreasing trend, which is non null up to 3300 m. However, for both the relative decrease and the percentage of massifs with a decreasing trend, even if we notice a similar declining pattern, we also detect a slight growth above 3000 m. This echoes results from Lüthi et al. (2019), which found that, in the Alps above 3000 m, the

205   relative decrease for projected winter-mean of fresh snow water equivalent is more marked than at 3000 m (see their Figure 8). We emphasize, however, that most meteorological observations used as input to the SAFRAN-Crocus reanalysis are situated below 2000 m. Therefore, trends beyond 2000 m altitude should be considered with great caution.

Figure 7 illustrates that, for altitudes 300 m and 600 m, in general no trend are found except few decreasing trends at 600 m and 3 time series (1 at 300 m, 2 at 600 m) with sometimes important increasing trends (+100% for the Parpaillon massif at

210   600 m). Despite this important increase in relative change, recorded annual maxima of snow load remain small (< 1 kN m^{-2}). Indeed, we found that these annual maxima correspond to snow load accumulated in few days, and thus are mainly driven by heavy precipitations rather than a full season snowpack accumulation. In particular, we hypothesize that the 2 massifs with important increasing trends (red color) might be caused by a local phenomenon called "East return" which is a low pressure system coming from the Mediterranean sea, that might be intensifying with global warming (Garavaglia et al., 2010; Faranda,

215   2019).

To sum up trends in return levels of ground snow load: from 900 m to 4800 m, either no trend or decreasing trend of 50-year return levels of GSL are found (Fig. 5, Fig. 6 and Fig. A1). while at 300 m and 600 m, no clear trends are found (Fig. 7).
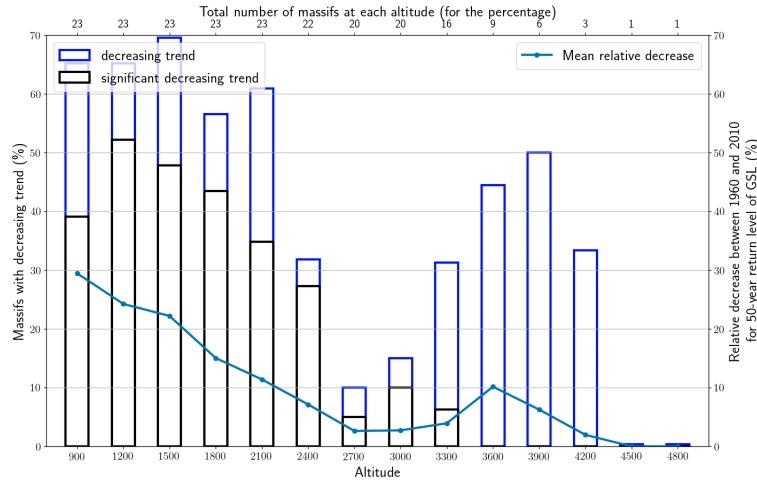
Figure 6. Temporal decreasing trend of 50-year return levels of ground snow load (GSL) between 900 m and 4800 m of altitude.
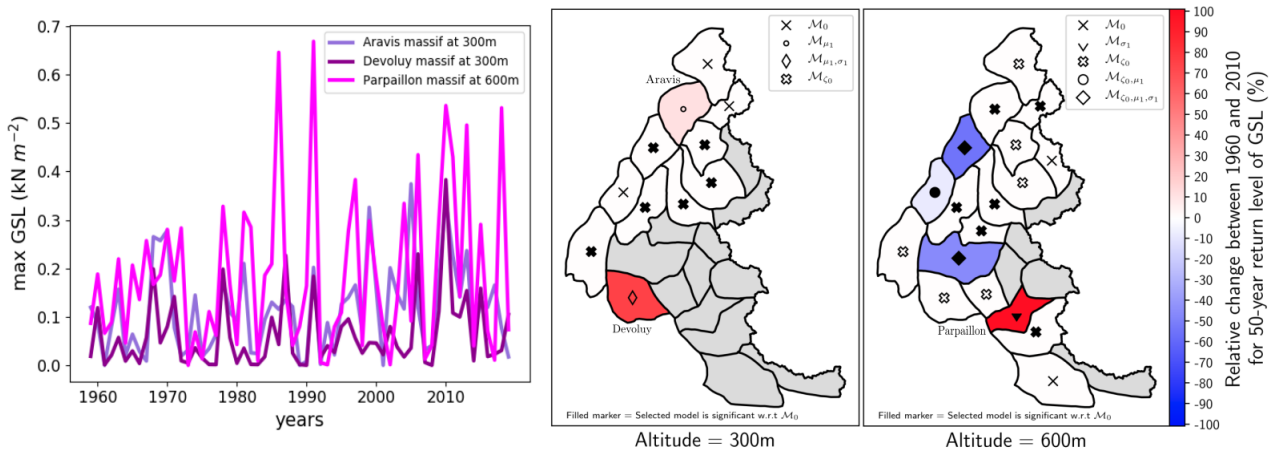

Figure 7. Left: Time series of annual maxima for ground snow load (GSL) for 3 massifs either at 300 m or 600 m of altitude. Right: Trend for annual maxima of ground snow load (GSL) at 300 m and 600 m of altitude. Markers show selected model $\mathcal{M}_N$.

5.3 Comparison of return levels of ground snow load with French standards

Every 300 m of altitude, from 300 m to 1800 m, we compute 50-year return levels and their uncertainty from GSL data (Sect. 4.3), and compare them to French standards (Sect. 3) for the 23 French Alps massifs.

Figure 8 illustrates these levels and their uncertainty for two massifs (Vercors and Beaufortain) associated to different French standards regions. Standards are often exceeded at higher altitudes (e.g. at 1800 m). Also, Figure 8 exemplifies the impact of accounting for decreasing trends in return levels. Indeed, we observe that return levels from the stationary Gumbel model $\mathcal{M}_0$ (Left) are often above effective return levels in 2019 (last year of data) from the selected model $\mathcal{M}_N$ (Right).

11

225   Figure 9 sums up the comparison between French standards and our results. We display the percentage of massifs whose
return level estimated from data exceeds return level from standards. The number of massifs with available data is equal to
11 at 300 m, 18 at 600 m, and 23 at 900 m and above. Limits of the confidence intervals (black bars) are computed as the
percentage of exceedances for the limits of return levels' 95% confidence interval (black bars on Fig. 8)..

First, if we estimate return levels from data with French standards method (Fig. 9 Left), i.e. with a stationary Gumbel model
230    $\mathcal{M}_0$, and GSL data approximated with snow depth obtained from reanalysis and $\rho_{\mathrm{SNOW}} = 150 \ \mathrm{kg \ m^{-3}}$, then we observe few
exceedances (always less than 10%). Thus, in this setting, estimations from our reanalysis are consistent with French standards.

However, if we consider the actual GSL, i.e. computed with the snow water equivalent from reanalysis, then French standards
drastically underestimate return levels. Indeed, with a stationary Gumbel model $\mathcal{M}_0$, then for altitudes above or equal to 900
m, French standards are exceeded for a majority of massifs (Fig. 9 Center). But, if we consider the selected model $\mathcal{M}_N$, i.e.
235   if we account for the decreasing trend in 50-year return levels, we have less exceedances at all altitudes (Fig. 9 Right). In the
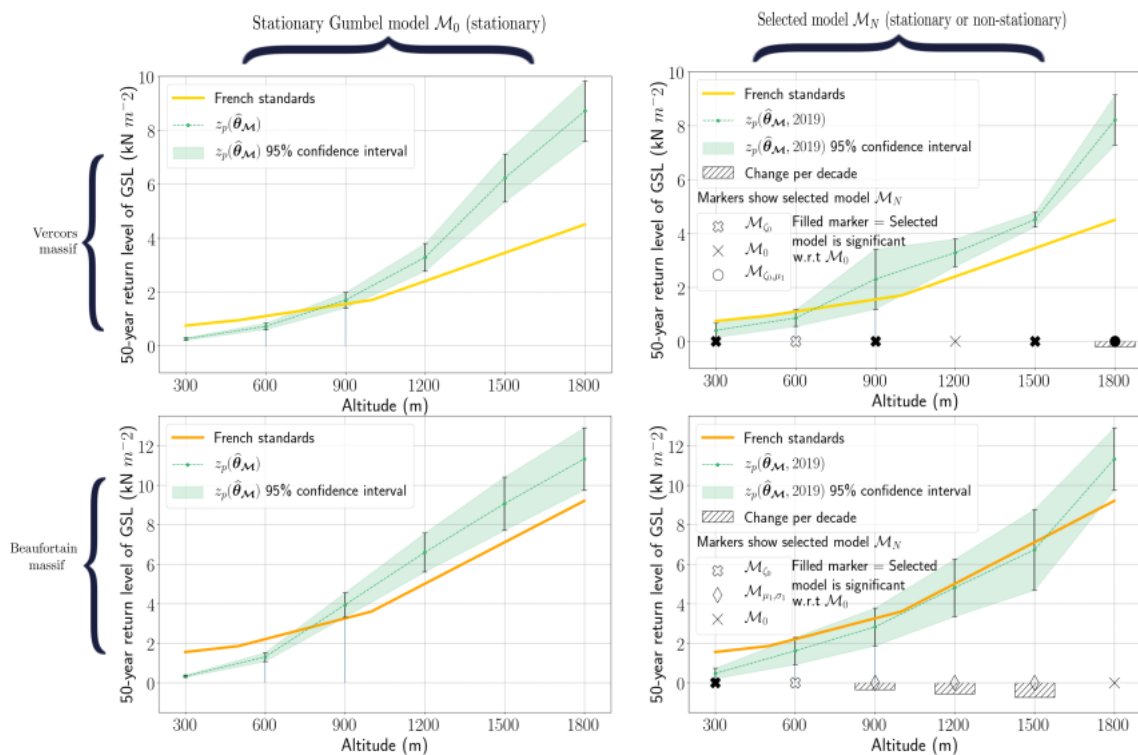latter case, at worst, i.e. at 1800 m, half of the massifs still exceed French standards return levels.

Figure 8. 50-year return levels of ground snow load (GSL) from altitude 300 m to 1800 m for Vercors (Top) and Beaufortain (Bottom)
massifs. Return levels (green line) and their uncertainty (shaded green and black bars) are estimated from the data either with the stationary
Gumbel model $\mathcal{M}_0$ (Left) or with the selected model $\mathcal{M}_N$ (Right). If $\mathcal{M}_N$ is a non-stationary model, return level is the effective return level
in 2019, and we display the change in return level per decade (striped histogram), i.e. 10 times the time derivative of return level (Sect. 4.3).
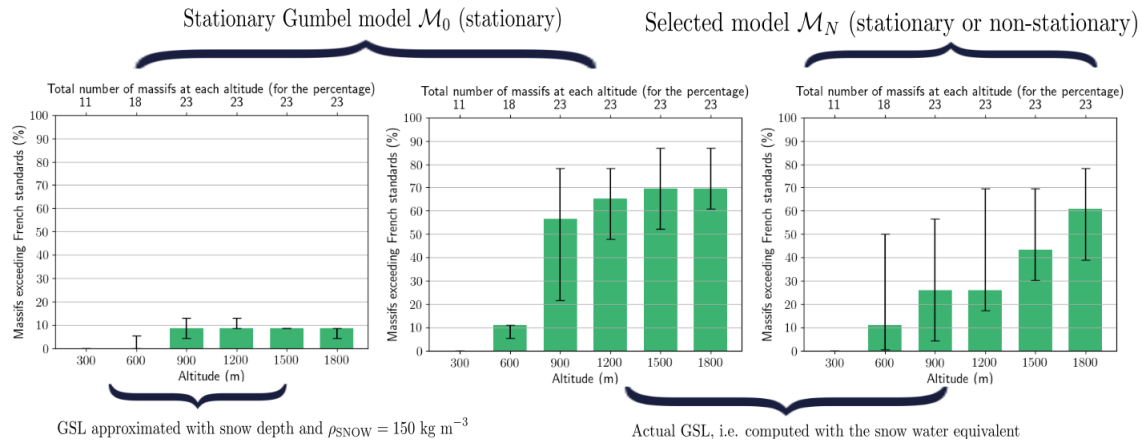
Figure 9. Percentage of massifs (green histogram) whose 50-year return levels of ground snow load (GSL) is above French standards between 300 m and 1800 m. Uncertainty (black bars) is approximated as the percentage of exceedances for return levels' 95% confidence interval limits. Left: similar to French standard estimation (stationary Gumbel $\mathcal{M}_0$, and GSL approximated with snow depth obtained from reanalysis and $\rho_{\mathrm{SNOW}} = 150\ \mathrm{kg\ m^{-3}}$). Center: stationary Gumbel $\mathcal{M}_0$, and actual GSL, i.e. computed with the snow water equivalent from reanalysis. Right: selected model $\mathcal{M}_N$ (if $\mathcal{M}_N$ is non-stationary, return level is the effective return level in 2019) and actual GSL.

6 Discussion

6.1 Methodological considerations

We discuss in depth the statistical models chosen for this study. It is well-known that an annual maximum based approach
240   can be wasteful in terms of data (Coles, 2001). However, since our objective is to estimate 50-year return levels and since we have 60 years of data, we still decide to rely on the annual maximum based approach (with the GEV distribution) rather than on the concurrent approach based on threshold exceedances (with the Generalized Pareto distribution). Also, with the GEV distribution (and its particular case: the Gumbel distribution) our methodology is a direct extension of French building standards (Sect. 3).

245   For the non-stationary models, we focus on simple deterministic function of time $(\mu(t), \sigma(t), \zeta(t))$ due to the limited length of time series. A linear non-stationarity seems preferable to a non-stationarity based on the Heaviside step function due to the continuous nature of climate change. We start the linear non-stationary at the initial year, i.e. 1959. We tried to start the non-stationarity only after a most likely year (Blanchet et al., 2016) but our results lacked coherence both between close massifs (no clear spatial pattern for the most likely years) and w.r.t. the altitude (no clear trend in most likely years as altitude rises).

250   We decided to consider non-stationarity only for the location and scale parameter. Indeed, in the literature, a linear non-stationarity is considered sometimes only for the location parameter (Fowler et al., 2010; Tramblay and Somot, 2018) but more often both for the location and the scale (or log-transformed scale for numerical reasons) parameters (Katz et al., 2002; Kharin and Zwiers, 2004; Marty and Blanchet, 2012; Wilcox et al., 2018). Another reason for which we considered a non-stationarity

for both parameters is that we did not find the scale parameters to be proportional to the location parameters, which could have

255 otherwise simplified our parametrization. Also, the shape parameter is typically considered constant, with few exceptions in the literature and we follow this approach.

For time series containing zeros, French standards rely on a mixed discrete-continuous distribution. We did not rely on this choice because for time series containing zeros considered in this study, i.e. with less than 10% of zeros (Sect. 5), we almost obtain the same 50-year return levels with this distribution than with our approach (absolute difference remains lower than

260 0.1 kN m^{-2}).

6.2 On the limitation to approximate annual maxima of ground snow load with annual maxima of snow depth

Snow water equivalent (SWE) times the gravitational constant equals GSL. However, most countries do not measure SWE but only have access to snow depth (HS) (Haberkorn et al., 2019). In that case, snow density is required to obtain SWE (and subsequently GSL) from HS (Sect. 1). In particular, French standards approximate annual maxima of GSL with annual maxima

265 of HS and by assuming a constant snow density, equal to $\rho_{\mathrm{SNOW}} = 150$ kg m^{-3}. We highlight limitations of such approaches with our reanalysis (Sect. 2) that provides, for the whole snowpack, daily values of SWE, HS, and thus of snow density.

We find that annual maxima of GSL is always underestimated by French standards' approximation (Fig. 10 Left). Main reason is that, when annual maxima of GSL is reached, snow density is in average largely superior to $\rho_{\mathrm{SNOW}} = 150$ kg m^{-3} (Fig. 10 Center). Indeed, we observe that at the time of the annual maxima of GSL the snow density is around ≈ 350 kg m^{-3}

270 in average at 2700 m, and close to ≈ 250 kg m^{-3} in average at 900 m. Finally, despite high variations along the years, we also notice that, when annual maxima of GSL is reached, snow depth can be much lower than the annual maxima of snow depth (Fig. 10 Right), which is another argument against the use of snow depth maxima as a proxy for GSL maxima.
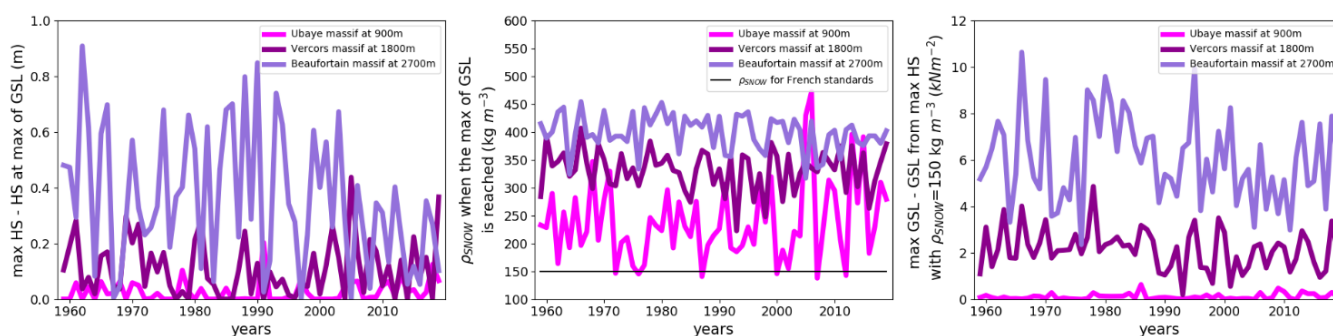

Figure 10. Limitation of approximating annual maxima of ground snow load (GSL) from annual maxima of snow depth (HS). Left: Difference between annual maxima of GSL and GSL computed from annual maxima of HS and $\rho_{\mathrm{SNOW}} = 150$ kg m^{-3}. Center: Snow density when annual maxima of GSL is reached. Right: Difference between annual maxima of HS and HS when annual maxima of GSL is reached.

Natural Hazards
and Earth System
Sciences

Discussions

EGU

7   Conclusions

Based on both a reanalysis and a snowpack model, we detect an overall temporal decreasing trend w.r.t to 50-year return levels
275   of ground snow load (GSL) between 900 m and 4200 m, which is significant until 2100 m in the Northwest of the French Alps.
This confirms other studies in the Western Alps which also found overall decreasing trends in linked snowpack variables: snow
water equivalent and snow depth. Despite decreasing return levels, in half of the massifs the 50-year return level in 2019 at
1800 m exceeds the stationary return level designed for French standards.

We hypothesize that this amount of exceedances might be due to an underestimation of GSL by French standards. Indeed,
280   these standards were devised with GSL estimated from snow depth and constant snow density equal to $150\,\mathrm{kg\,m^{-3}}$, which
underestimate typical GSL values for the full snowpack. Another reason for these exceedances might be ill-designed relation-
ships between altitude and snow load. As shown on Fig. 2, French standards return levels augment linearly by parts w.r.t the
altitude. Indeed, French standards (Biétry, 2005) follow previous national standards (AFNOR, 1996) that advised for a linear
relationship between altitude and snow load instead of relying on European standards' results that showed a quadratic relation-
285   ship for the Alpine Region (Sanpaolesi et al., 1998). Thus, at higher altitudes, French standards might underestimate actual
return levels which might explain the augmenting percentage of exceedance that we observe w.r.t the altitude (Fig. 9 Right).

Many potential extensions of this work could be considered. First, our methodology could be extended with more advanced
definitions of non-stationary return levels (Rootzén and Katz, 2013; Serinaldi, 2015). Also, instead of considering time series of
annual maxima as independent, we believe that our analysis may benefit from an explicit modelling of the spatial dependence
290   between extremes. Then, reanalyses are increasingly available at the European scale (e.g. Soci et al. (2016)), which could be
used for extending this work at a wider geographical scale. This requires, however, to remain cognizant of the limitations of
such reanalyses, in particular (i) the temporal heterogeneity of the meteorological data input to these reanalyses (Vidal et al.,
2010), (ii) the lack of observations at high elevations, requiring caution in analyzing trends for high elevation locations and
(iii) model errors (e.g., snowpack model errors) which need to be taken into account when analyzing the results.

295   Finally, even if, according to our analysis, GSL exceeds French standards return levels in the French Alps, (Fig. 9 Right),
few destructions related to snow loads actually occurred. Several reasons might explain that. First, French standards consider a
coefficient that maps GSL return levels to roof snow load return level, i.e. multiplication by a coefficient that summarizes several
roof features: shape, exposure and thermal transmission (Sanpaolesi et al., 1998)). This coefficient might be overprotective.
Also, following European standards, to ensure roofs reliability, designers actually build roofs that withstand return levels of
300   roof snow load multiplied by a safety coefficient (1.5). Above all, French standards do not take into account that, after intense
days of snowfall, the snow accumulated on the roof either slides off or is removed. In that case, the main risk lies in extreme
snow events that might accumulate in few days enough snow to exceed French standards. Undeniably, most known snow load
destructions resulted from such intense snow events, sometimes combined with liquid precipitation that often heavily increase
snow load. The response of these short but extreme and complex snow events to climate change might be an interesting topic
305   for future research.

Author contributions. E.L.R performed the analysis and drafted the first version of the manuscript. All authors discussed the results and edited the manuscript.

Competing interests. The authors declare that they have no conflict of interest.

Data availability. Dataset can be download from AERIS website https://www.aeris-data.fr/catalogue/ (type "S2M" in the search bar).

Appendix A: Trends in return levels of ground snow load

In this section, we report, for every 300 m of altitude from 900 m to 4200 m, the map of the relative change between 1960 and
315   2010 for the 50-year return levels of GSL (Fig. A1). Trends at 4500 m and 4800 m are not reported, since they only concern the Mont Blanc massif, where no significant trend is inferred at these altitudes.
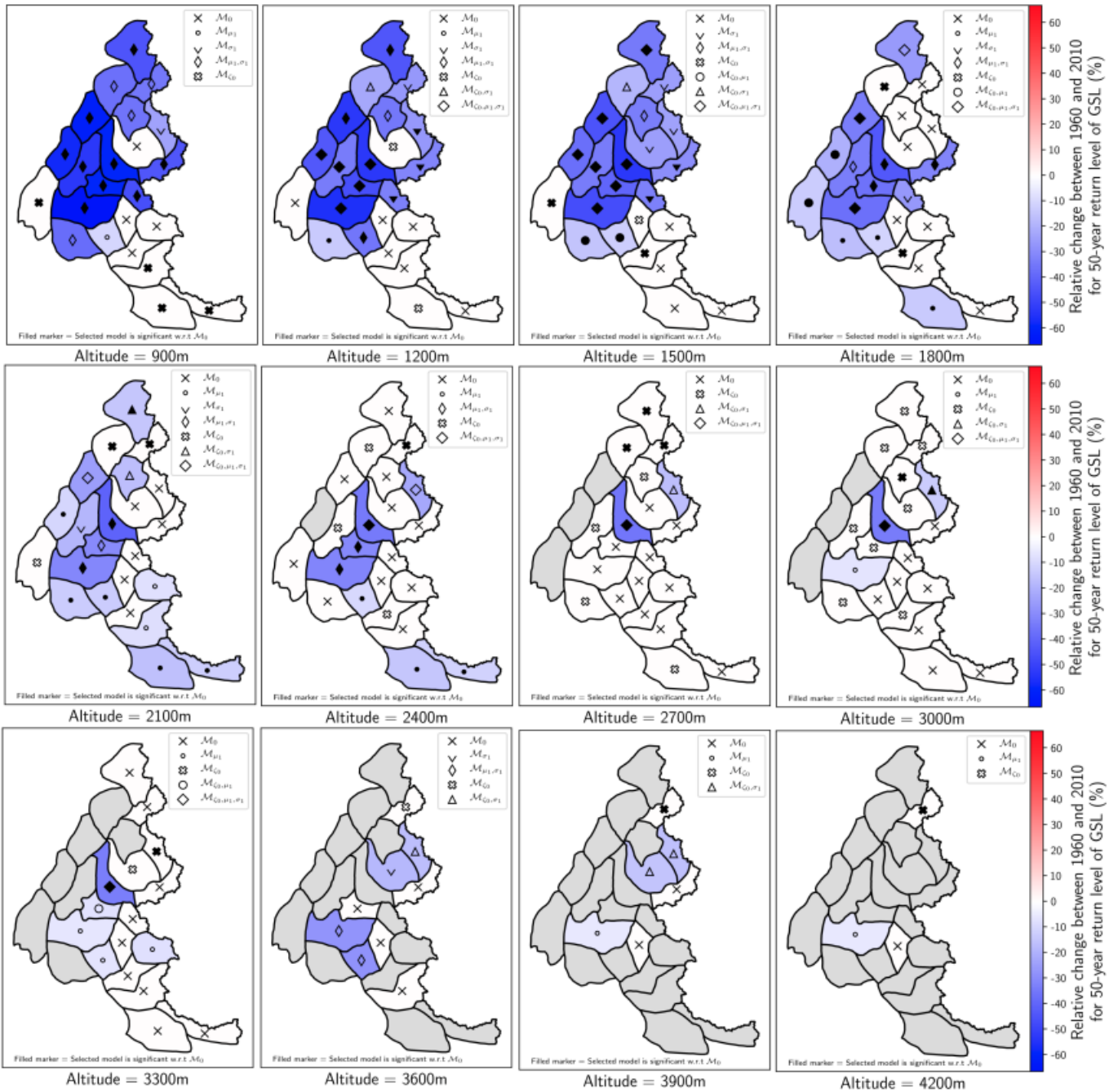
Natural Hazards
and Earth System
Sciences
Discussions
Open Access
EGU

Figure A1. Trends in return levels of ground snow load (GSL) between 900 m and 4200 m of altitude. Markers show selected model $\mathcal{M}_N$.

Natural Hazards
and Earth System
Sciences
Discussions

Open Access

EGU

References

AFNOR: DTU P06 006, Tech. rep., AFNOR, 1996.

Akaike, H.: A New Look at the Statistical Model Identification, IEEE transactions on automatic control, pp. 215–222,
320   https://doi.org/10.1007/978-1-4612-1694-0_16, 1974.

BBC News: Arrests over Poland roof collapse, http://news.bbc.co.uk/2/hi/europe/5119424.stm, 2006.

Beniston, M., Farinotti, D., Stoffel, M., Andreassen, L. M., Coppola, E., Eckert, N., Fantini, A., Giacona, F., Hauck, C., Huss, M., Huwald,
H., Lehning, M., López-Moreno, J.-I., Magnusson, J., Marty, C., Terzago, S., and Vincent, C.: The European mountain cryosphere: a
review of its current state, trends, and future challenges, The Cryosphere, 12, 759–794, https://doi.org/10.5194/tc-12-759-2018, 2018.

325   Biétry, J.: Charges de neige au sol en France : proposition de carte révisée, Tech. Rep. 0, groupe de travail « Neige » de la commission de
normalisation BNTEC P06A, 2005.

Blanchet, J., Molinié, G., and Touati, J.: Spatial analysis of trend in extreme daily rainfall in southern France, Climate Dynamics, 51, 799–
812, https://doi.org/10.1007/s00382-016-3122-7, 2016.

Bocchiola, D. and Diolaiuti, G.: Evidence of climate change within the Adamello Glacier of Italy, Theoretical and Applied Climatology,
330   100, 351–369, https://doi.org/10.1007/s00704-009-0186-x, 2010.

Cheng, L., AghaKouchak, A., Gilleland, E., and Katz, R. W.: Non-stationary extreme value analysis in a changing climate, Climatic Change,
127, 353–369, https://doi.org/10.1007/s10584-014-1254-5, 2014.

Coles, S. G.: An introduction to Statistical Modeling of Extreme Values, Springer Series in Statistics, p. 221, https://doi.org/10.1007/978-1-
4471-3675-0, 2001.

335   Cooley, D.: Return Periods and Return Levels Under Climate Change, in: Extremes in a Changing Climate - Detection, Analysis & Uncer-
tainty, pp. 97–114, Springer Science & Business Media, 2012.

Croce, P., Formichi, P., Landi, F., Mercogliano, P., Bucchignani, E., Dosio, A., and Dimova, S.: The snow load in Europe and the climate
change, Climate Risk Management, 20, 138–154, https://doi.org/10.1016/j.crm.2018.03.001, 2018.

Durand, Y., Laternser, M., Giraud, G., Etchevers, P., Lesaffre, B., and Mérindol, L.: Reanalysis of 44 yr of climate in the French Alps (1958-
340   2002): Methodology, model validation, climatology, and trends for air temperature and precipitation, Journal of Applied Meteorology and
Climatology, 48, 429–449, https://doi.org/10.1175/2008JAMC1808.1, 2009a.

Durand, Y., Rald Giraud, G., Laternser, M., Etchevers, P., Mé Rindol, L., and Lesaffre, B.: Reanalysis of 47 Years of Climate
in the French Alps (1958–2005): Climatology and Trends for Snow Cover, Journal of applied meteorology and climatology,
https://doi.org/10.1175/2009JAMC1810.1, 2009b.

345   Faranda, D.: An attempt to explain recent trends in European snowfall extremes (Preprint), Weather and Climate Dynamics, 2019.

Fisher, R. A. and Tippett, L. H. C.: Limiting forms of the frequency distribution of the largest or smallest member of a sample, Mathematical
Proceedings of the Cambridge Philosophical Society, 24, 180, https://doi.org/10.1017/S0305004100015681, 1928.

Fowler, H. J., Cooley, D., Sain, S. R., and Thurston, M.: Detecting change in UK extreme precipitation using results from the climatepredic-
tion.net BBC climate change experiment, Extremes, 13, 241–267, https://doi.org/10.1007/s10687-010-0101-y, 2010.

350   G Klein Tank, A. M. and K Nnen, G. P.: Trends in Indices of Daily Temperature and Precipitation Extremes in Europe, 1946–99, Journal of
Climate, 2003.

Garavaglia, F., Gailhard, J., Paquet, E., Lang, M., Garçon, R., and Bernardara, P.: Introducing a rainfall compound distribution model based
on weather patterns sub-sampling, Hydrology and Earth System Sciences, 14, 951–964, https://doi.org/10.5194/hess-14-951-2010, 2010.

Natural Hazards
and Earth System
Sciences
Discussions

Gaume, J., Chambon, G., Eckert, N., and Naaim, M.: Relative influence of mechanical and meteorological factors on avalanche release depth
distributions: An application to French Alps, Geophysical Research Letters, 39, 1–5, https://doi.org/10.1029/2012GL051917, 2012.

Gaume, J., Eckert, N., Chambon, G., Naaim, M., and Bel, L.: Mapping extreme snowfalls in the French Alps using max-stable processes,
Water Resources Research, 49, 1079–1098, http://doi.wiley.com/10.1002/wrcr.20083, 2013.

Gilleland, E. and Katz, R. W.: extRemes 2.0: An Extreme Value Analysis Package in R, Journal of Statistical Software, 72, 1–39,
https://doi.org/10.18637/jss.v072.i08, 2016.

Gnedenko, B.: Sur la distribution limite du terme maximum d'une série aléatoire, The Annals of Mathematics, 44, 423,
https://doi.org/10.2307/1968974, 1943.

Haberkorn, A., Helmert, J., Leppänen, L., López-Moreno, J. I., and Pirazzini, R.: European Snow Booklet, 2019.

Il Jeong, D. and Sushama, L.: Projected changes to extreme wind and snow environmental loads for buildings and infrastructure across
Canada, Sustainable Cities and Society, 36, 225–236, https://doi.org/10.1016/J.SCS.2017.10.004, 2018.

IPCC: Managing the risks of extreme events and disasters to advance climate change adaptation, Cambridge University Press,
https://doi.org/10.1596/978-0-8213-8845-7, 2012.

IPCC: Special Report: The Ocean and Cryosphere in a Changing Climate, In press, https://doi.org/https://www.ipcc.ch/report/srocc/, 2019.

Katz, R. W., Parlange, M. B., and Naveau, P.: Statistics of extremes in hydrology, Advances in Water Resources, 25, 1287–1304,
https://doi.org/10.1016/S0309-1708(02)00056-8, 2002.

Kharin, V. V. and Zwiers, F. W.: Estimating extremes in transient climate change simulations, Journal of Climate, 18, 1156–1173,
https://doi.org/10.1175/JCLI3320.1, 2004.

Kim, H., Kim, S., Shin, H., and Heo, J. H.: Appropriate model selection methods for nonstationary generalized extreme value models, Journal
of Hydrology, 547, 557–574, https://doi.org/10.1016/j.jhydrol.2017.02.005, http://dx.doi.org/10.1016/j.jhydrol.2017.02.005, 2017.

Krinner, G., Derksen, C., Essery, R., Flanner, M., Hagemann, S., Clark, M., Hall, A., Rott, H., Brutel-Vuilmet, C., Kim, H., Ménard, C. B.,
Mudryk, L., Thackeray, C., Wang, L., Arduini, G., Balsamo, G., Bartlett, P., Boike, J., Boone, A., Chéruy, F., Colin, J., Cuntz, M., Dai, Y.,
Decharme, B., Derry, J., Ducharne, A., Dutra, E., Fang, X., Fierz, C., Ghattas, J., Gusev, Y., Haverd, V., Kontu, A., Lafaysse, M., Law, R.,
Lawrence, D., Li, W., Marke, T., Marks, D., Ménégoz, M., Nasonova, O., Nitta, T., Niwano, M., Pomeroy, J., Raleigh, M. S., Schaedler,
G., Semenov, V., Smirnova, T. G., Stacke, T., Strasser, U., Svenson, S., Turkov, D., Wang, T., Wever, N., Yuan, H., Zhou, W., and Zhu,
D.: ESM-SnowMIP: Assessing snow models and quantifying snow-related climate feedbacks, Geoscientific Model Development, 11,
5027–5049, https://doi.org/10.5194/gmd-11-5027-2018, 2018.

Laternser, M. and Schneebeli, M.: Long-term snow climate trends of the Swiss Alps (1931-99), International Journal of Climatology, 23,
733–750, https://doi.org/10.1002/joc.912, 2003.

Lüthi, S., Ban, N., Kotlarski, S., Steger, C. R., Jonas, T., and Schär, C.: Projections of Alpine snow-cover in a high-resolution climate
simulation, Atmosphere, 10, 1–18, https://doi.org/10.3390/atmos10080463, 2019.

Martins, E. S. and Stedinger, J. R.: Generalized maximum-likelihood generalized extreme-value quantile estimators for hydrologic data,
Water Resources Research, 36, 737–744, https://doi.org/10.1029/1999WR900330, 2000.

Marty, C. and Blanchet, J.: Long-term changes in annual maximum snow depth and snowfall in Switzerland based on extreme value statistics,
Climatic Change, 111, 705–721, https://doi.org/10.1007/s10584-011-0159-9, 2012.

Marty, C., Tilg, A.-M., Jonas, T., Marty, C., Tilg, A.-M., and Jonas, T.: Recent Evidence of Large-Scale Receding Snow Water Equivalents
in the European Alps, Journal of Hydrometeorology, 18, 1021–1031, https://doi.org/10.1175/JHM-D-16-0188.1, 2017.

Natural Hazards
and Earth System
Sciences
Discussions
EGU
Open Access

Milly, P. C. D., Bentacourt, J., Falkenmark, M., Robert, M., Hirsch, R. M., Kundzewicz, Z. W., Letternmaier, D. P., and Stouffer, R. J.: Stationarity is dead: Whither water management? , Science, 319, 573–574, 2008.

Montanari, A. and Koutsoyiannis, D.: Modeling and mitigating natural hazards: Stationarity is immortal!, Water Resources Research, 50, 9748–9756, https://doi.org/10.1002/2014WR016092, 2014.

395 Mortimer, C., Mudryk, L., Derksen, C., Luojus, K., Brown, R., Kelly, R., and Tedesco, M.: Evaluation of long term Northern Hemisphere snow water equivalent products, The Cryosphere Discussions, submitted, 1–24, 2019.

Naaim-Bouvet, F., Prat, M., Jacob, J., Calgaro, J. A., and & Raoul, J.: La neige : recherche et réglementation, Presses de l'École nationale des ponts et chaussées, 2000.

Nicolet, G., Eckert, N., Morin, S., and Blanchet, J.: Inferring Spatio-temporal Patterns in Extreme Snowfall in the French Alps Using Max-
400 stable Processes, Procedia Environmental Sciences, 27, 75–82, https://doi.org/10.1016/j.proenv.2015.07.102, 2015.

Nicolet, G., Eckert, N., Morin, S., and Blanchet, J.: Decreasing spatial dependence in extreme snowfall in the French Alps since 1958 under climate change, Journal of Geophysical Research, 121, 8297–8310, https://doi.org/10.1002/2016JD025427, 2016.

Nicolet, G., Eckert, N., Morin, S., and Blanchet, J.: A multi-criteria leave-two-out cross-validation procedure for max-stable process selection, Spatial Statistics, 22, 107–128, https://doi.org/10.1016/j.spasta.2017.09.004, https://doi.org/10.1016/j.spasta.2017.09.004, 2017.

405 Nicolet, G., Eckert, N., Morin, S., and Blanchet, J.: Assessing Climate Change Impact on the Spatial Dependence of Extreme Snow Depth Maxima in the French Alps, Water Resources Research, 54, 7820–7840, https://doi.org/10.1029/2018WR022763, https://onlinelibrary.wiley.com/doi/abs/10.1029/2018WR022763, 2018.

O'Rourke, M. and Auren, M.: Snow loads on gable roofs, Journal of Structural Engineering, 123, 1645–1651, https://doi.org/10.1061/(ASCE)0733-9445(1997)123:12(1645), 1997.

410 Rajczak, J. and Schär, C.: Projections of Future Precipitation Extremes Over Europe: A Multimodel Assessment of Climate Simulations, Journal of Geophysical Research: Atmospheres, 122, 773–10, https://doi.org/10.1002/2017JD027176, 2017.

Rootzén, H. and Katz, R. W.: Design Life Level: Quantifying risk in a changing climate, Water Resources Research, 49, 5964–5972, https://doi.org/10.1002/wrcr.20425, 2013.

Rózsás, A., Sýkora, M., and Vigh, L. G.: Long-Term Trends in Annual Ground Snow Maxima for the Carpathian Region, Applied Mechanics
415 and Materials, 821, 753–760, https://doi.org/10.4028/www.scientific.net/amm.821.753, 2016.

Sanpaolesi, L., Currie, D., Sims, P., Sacre, C., Stiefel, U., Lozza, S., Eiselt, B., Peckham, R., Solomos, G., Holand, I., et al.: Scientific support activity in the field of structural stability of civil engineering works: snow loads, Final Report Phase I. Brussels: Commission of the European Communities. DGIII-D3, 1998.

Schöner, W., Koch, R., Matulla, C., Marty, C., and Tilg, A. M.: Spatiotemporal patterns of snow depth within the Swiss-Austrian
420 Alps for the past half century (1961 to 2012) and linkages to climate change, International Journal of Climatology, 39, 1589–1603, https://doi.org/10.1002/joc.5902, 2019.

Serinaldi, F.: Dismissing return periods!, Stochastic Environmental Research and Risk Assessment, 29, 1179–1189, https://doi.org/10.1007/s00477-014-0916-1, 2015.

Serinaldi, F. and Kilsby, C. G.: Stationarity is undead: Uncertainty dominates the distribution of extremes, Advances in Water Resources, 77,
425 17–36, https://doi.org/10.1016/J.ADVWATRES.2014.12.013, 2015.

Soci, C., Bazile, E., Besson, F. O., and Landelius, T.: High-resolution precipitation re-analysis system for climatological purposes, Tellus, Series A: Dynamic Meteorology and Oceanography, 68, https://doi.org/10.3402/tellusa.v68.29879, 2016.

Natural Hazards
and Earth System
Sciences
Discussions

Strasser, U.: Snow loads in a changing climate: New risks?, Natural Hazards and Earth System Science, 8, 1–8, https://doi.org/10.5194/nhess-8-1-2008, 2008.

430   Terzago, S., Fratianni, S., and Cremonini, R.: Winter precipitation in Western Italian Alps (1926–2010), Meteorology and Atmospheric Physics, 119, 125–136, https://doi.org/10.1007/s00703-012-0231-7, 2013.

Tramblay, Y. and Somot, S.: Future evolution of extreme precipitation in the Mediterranean, Climatic Change, https://doi.org/10.1007/s10584-018-2300-5, 2018.

Vernay, M., Lafaysse, M., Hagenmuller, P., Nheili, R., Verfaillie, D., and Morin, S.: The S2M meteorological and snow cover reanalysis in
435   the French mountainous areas (1958 - present), [Data set]. AERIS, https://doi.org/https://doi.org/10.25326/37, 2019.

Vidal, J. P., Martin, E., Franchistéguy, L., Baillon, M., and Soubeyroux, J. M.: A 50-year high-resolution atmospheric reanalysis over France with the Safran system, International Journal of Climatology, 30, 1627–1644, https://doi.org/10.1002/joc.2003, 2010.

Vigneau, J.-P.: 1986 dans les Pyrénées orientales : deux perturbations méditerranéennes aux effets remarquables, Revue géographique des Pyrénées et du Sud-Ouest, 58, 23–54, https://doi.org/10.3406/rgpso.1987.4969, 1987.

440   Vionnet, V., Brun, E., Morin, S., Boone, A., Faroux, S., Le Moigne, P., Martin, E., and Willemet, J.-M.: Geoscientific Model Development The detailed snowpack scheme Crocus and its implementation in SURFEX v7.2, Geosci. Model Dev, 5, 773–791, https://doi.org/10.5194/gmd-5-773-2012, 2012.

Wilcox, C., Vischel, T., Panthou, G., Bodian, A., Blanchet, J., Descroix, L., Quantin, G., Cassé, C., Tanimoun, B., and Kone, S.: Trends in hydrological extremes in the Senegal and Niger Rivers, Journal of Hydrology, 566, 531–545,
445   https://doi.org/10.1016/J.JHYDROL.2018.07.063, 2018.

Zhang, X., Zwiers, F. W., Li, G., Zhang, X., Zwiers, F. W., and Li, G.: Monte Carlo Experiments on the Detection of Trends in Extreme Values, Journal of Climate, 17, 1945–1952, https://doi.org/10.1175/1520-0442(2004)017<1945:MCEOTD>2.0.CO;2, 2004.